Available online at www.sciencedirect.com

ScienceDirect

Proceedings of the Combustion Institute 36 (2017) 2761–2769

Proceedings of the Combustion Institute

www.elsevier.com/locate/proci

Wedge-stabilized oblique detonation in an inhomogeneous hydrogen–air mixture

Kazuya Iwata*, Shinji Nakaya, Mitsuhiro Tsue

Department of Aeronautical and Astronautical Engineering, School of Engineering, University of Tokyo, Hongo 7-3-1, Bunkyo-ku, Tokyo 113-8656, Japan

Received 4 December 2015; accepted 11 June 2016
Available online 22 June 2016

Abstract

We performed numerical simulation against oblique detonation formed in an inhomogeneous hydrogen–air mixture. Planar two-dimensional Navier–Stokes equations were solved with the chemical source terms calculated with a detailed chemical kinetics including 9 species and 27 elementary reactions. Fuel concentration gradients described by the Gaussian function were introduced into two different conditions: (A) a Mach 8 flow onto a 28.20° wedge with a static pressure of 8.50 kPa, and (B) a Mach 8 flow onto a 23.8° wedge with a static pressure of 34.0 kPa. Fuel-rich conditions on the centerline generated V-shaped deflagration front under the former condition, and V + Y Mach stem under the latter due to the strong concentration gradients near the surface. These shapes caused a couple of triple points to appear on the incident shock front. Transition to detonation occurred twice along the front in some cases. The apex of V-shape was always located in a similar position due to almost constant thermochemical properties of the incoming streamline. The threshold for emergence of these V-shapes can be reasonably attained by the magnitude of induction length gradient close to the wedge.
© 2016 The Combustion Institute. Published by Elsevier Inc. All rights reserved.

Keywords: Oblique detonation; Shock-induced combustion; Hydrogen–air; Inhomogeneous; Non-uniform

1. Introduction

Oblique detonation wave (ODW) is a kind of supersonic combustion formed when a detonable mixture flows onto a solid body at a speed exceeding its Chapman–Jouguet (C–J) speed [1–3]. It has been studied extensively as a potential power source for conceptual hypersonic propulsion technologies such as an Oblique Detonation Wave Engine (ODWE) and a Ram Accelerator (RAMAC) [4–6]. Lehr [7] first observed ODW and shock-induced combustion (SIC, defined as combustion without interaction with the initiating shock wave) on a hypersonic spherical projectile by launching it into hydrogen–air and hydrogen–oxygen mixtures. Li et al. [8] performed a parametric numerical study on oblique detonation formed on a slip surface wedge, revealing the basic structure (Fig. 1) that consists of an inert oblique shock wave (OSW), an induction zone behind it followed by a deflagration front, and a detonation front downstream of the triple point

* Corresponding author.
E-mail addresses: 3138826900@mail.ecc.u-tokyo.ac.jp, something.violet666@gmail.com (K. Iwata).

http://dx.doi.org/10.1016/j.proci.2016.06.094
1540-7489 © 2016 The Combustion Institute. Published by Elsevier Inc. All rights reserved.

Nomenclature

a	steepness of the gradients
g	induction length gradient factor
H	position normal to the inflow
l_{ind}	induction length
x,y	Cartesian coordinates attached on the wedge
X	mole fraction
β	inert shock angle [°]
θ	half-wedge angle [°]
φ	equivalence ratio
Subscript	
0	centerline
s	outermost position

structure on which the deflagration front catches up with OSW.

Da Silva and Deshaies [9] also studied wedge-stabilized ODW under a wide range of inflow conditions numerically, classifying them by the transition pattern: the smooth-transition with a smooth increase of the shock angle through the OSW/ODW transition, and the abrupt-transition with a discontinuous increase. Choi et al. [10,11], Verreault et al. [12], and other researchers worked on the cellular structures on ODW which typically accompany normally propagating detonation. SIC with an oscillating flame front has also been analyzed by Matsuo and Fujii [13], Alpert and Toong [14]. Verreault and Higgins [15] experimentally investigated cone-induced ODW and SIC. Maeda et al. [16] observed and clarified the structures of Straw-Hat type ODW in their ballistic range experiment.

All of the works mentioned above and many other researches were concerned with homogeneously premixed mixtures [7–18]. Researches on ODW in fuel concentration gradients are rare [19–21], in contrast to the fact that normal detonation in the non-uniformity has been studied a lot [22–24]. Cambier et al. [19] simulated ODW in a couple of non-uniform conditions where local equivalence ratio was distributed by a pseudo-sinusoidal function from 1.90 on the centerline to 0.10 in the outermost location, and distributed according to the result of their mixing simulation of a pair of strut fuel injectors. They observed a strong curvature of the wave front due to the poor premixing in both conditions. Vlasenko and Sabel'nikov [20] also introduced the non-uniformity to an incoming mixture in their numerical simulation, observing a weak curvature on wedge-stabilized ODW front when incoming local equivalence ratio varied in a sinusoidal manner between 2.00 and 0.50. Sislian et al. [21] simulated the whole ODWE system with the non-uniform premixing described by the Gaussian distribution, revealing degradation of the engine performance. All the works mentioned above all concluded that the curvature of the front created by the variation of the incoming Mach number due to the non-uniform sound speed is the sole effect of the inhomogeneity. However, since the number of parameters chosen was limited to one or two, their physical insight into its structure was not comprehensive. When difficulty of the premixing in ODWE due to a hypersonic speed of the incoming air is considered, ODW in non-uniform mixtures must be studied in an extensive way to reveal the combustion characteristics and its effects on the performance of ODWE [21,25,26].

In the present paper, our work was mainly devoted to investigation of non-uniformly premixed ODW created by a hydrogen–air mixture formed on a solid wedge through a parametric numerical study. Two-dimensional numerical simulation was conducted to survey their structures.

2. Numerical simulation

In our study, characteristic features of wedge-stabilized oblique detonation formed in an inhomogeneous hydrogen–air mixture were addressed. We employed a rectangular-shaped computational domain which was attached on the surface of the wedge, as illustrated in Fig. 2.

A hypersonic premixed flow comes in from the left upper side of the domain at the half-wedge angle θ. Therefore, fixed inflow condition was imposed on the left and upper line. The right line is the outlet boundary on which a simple zero-gradient condition of the conserved quanti-

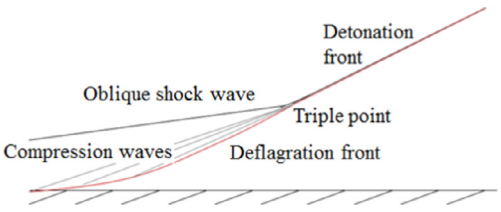

Fig. 1. Schematic picture of the basic structure of wedge-stabilized ODW.

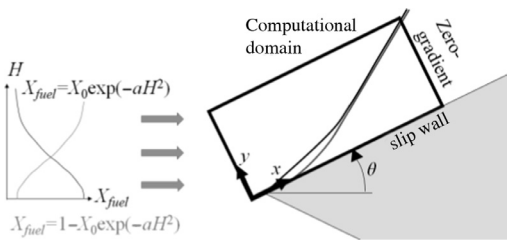

Fig. 2. Computational domain.

ties was used. The first 1.00 mm part of the lower line was also a zero-gradient outlet, and the rest was the surface of the wedge on which a slip-wall boundary condition was used. Effects of the boundary layer were not taken into account because our preliminary simulation revealed a negligible effect of it on the ODW structures obtained. There were three sizes of the grid employed: standard grid with 10.00 cm × 3.00 cm, extended grid with 12.50 cm × 3.00 cm, and largest grid with 15.00 cm × 3.00 cm. The resolution used was the same with $\Delta x = 125\,\mu$m and $\Delta y = 50\,\mu$m. Therefore, standard grid contains 801×601 grids, extended one 1001×601 grids, and largest one 1201×601 grids. About 10 grids were contained in the half reaction length of the completely premixed ODW which will be detailed later. This resolution is sufficient for calculation of ODW without any transversal waves as was confirmed by Teng et al. [18].

Two-dimensional Navier–Stokes equations were solved as the governing equations, involving 9 species continuity equations. The chemical source terms were calculated with a detailed reaction mechanism which was proposed and well validated by Konnov [27] which contains 27 elementary reactions.

Yee's second-order upwind TVD [28] was employed to discretize the convection terms, and the conventional second-order central difference was used to discretize the diffusive terms. Transport properties including viscosity, conductivity, and diffusion coefficient were calculated using the formulations by Chapman-Enskog et al. as summarized in [29], while the transport parameters (effective temperature and collision diameter) were derived online at the Web site of LLNL [30]. A fully implicit time integration method combining LU-SGS [31] and Point Implicit method [32] was used, by which only the steady state solutions were addressed. This implicit method was well validated by additional simulations with explicit time resolved methods revealing the absence of any unsteady motions of the shock fronts, the flame fronts and the triple point structures, which should be due to the absence of unstable transversal wave structures which Verreault et al. [12] predicted to appear at a lower degree of overdrive.

There are two conditions of the inflows considered in this study both of which were referred from the works by Da Silva and Deshaies [9]: (A) a Mach 8 flow onto a 28.20° wedge with a static pressure of 8.50 kPa, and (B) a Mach 8 flow onto a 23.80° wedge with a static pressure of 34.00 kPa. The former generated a smooth-transition ODW, and the latter generated an abrupt-transition ODW. The static temperature is 300 K for both conditions, and the mixture is uniformly stoichiometric composed of hydrogen and air. Concentration gradients were introduced into the above inflows, which were described using the Gaussian function as Eq. (1) below shows. The upper branch considers the most fuel-rich composition on the centerline (the center-rich condition), and the lower the most fuel-lean there (the center-lean condition). These distributions are justified by the measurements of hydrogen injected into supersonic flows [25,33].

Table 1
Incoming hydrogen concentration gradients in the present study.

Non-uniformity	φ_0	φ_s
1	1.50	0.44
2	2.00	0.24
3	2.50	0.15
4	3.00	0.09
5	4.00	0.05
6	5.00	0.03
7	6.00	0.02
8	7.00	0.01
9	8.00	0.01
10	0.50	1.84
11	0.25	3.72
12	0.13	4.63

$$X_{\mathrm{fuel}} = \begin{cases} X_{\mathrm{H_2},0} \exp(-aH^2) & \text{(Center-rich)} \\ 1 - X_{\mathrm{H_2},0} \exp(-aH^2) & \text{(Center-lean)} \end{cases} \quad (1)$$

H is the position vertical to the inflow with its origin on the apex of the wedge. Values of the two parameters X_0, a were chosen so that the total equivalence ratio computed from integration over the region $0 < H < Hs$ was kept unity, where Hs corresponds to the height of the intersection of the detonation front in the uniform conditions and the outlet boundary of standard grid. Nine non-uniform distributions were chosen in the above limitation, which are summarized in Table 1. φ_0 is the value on the centerline and φ_s is the value at $H = Hs$. The non-uniformities numbered 1–9 correspond to the center-rich conditions, and 10–12 to the center-lean conditions. The velocity, the static pressure and the static temperature were matched to the uniform cases. Hereafter, each computational case will be termed like 'Case A-1' according to the chosen inflow ((A) or (B)) and the chosen concentration gradient (from Table 1).

3. Results and discussion

3.1. Uniform conditions

Prior to the simulations of the non-uniform conditions on the wedge concerned, the completely premixed conditions with the inflows (A) and (B) described above were also simulated, and the results were compared with those by Da Silva and Deshaies [9]. Overlaid contours of pressure and water mass fraction as the results are shown in Fig. 3(a) and (b). Oblique arrows on the left upper side denote the direction of the incoming mix-

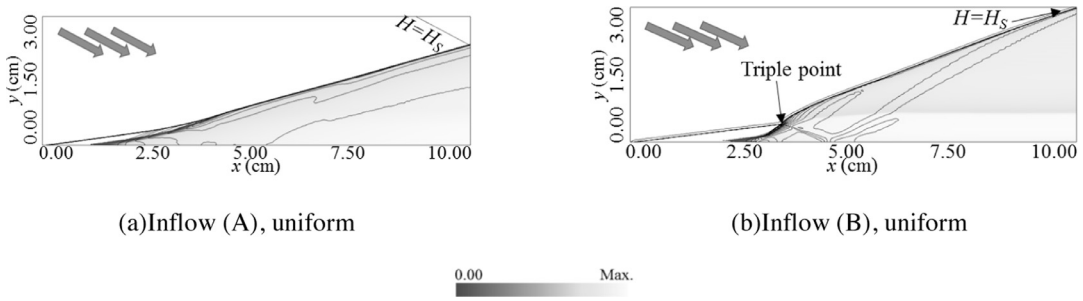

Fig. 3. Overlaid contours of pressure (black) and water mass fraction (gray–white) of the uniform conditions for validation.

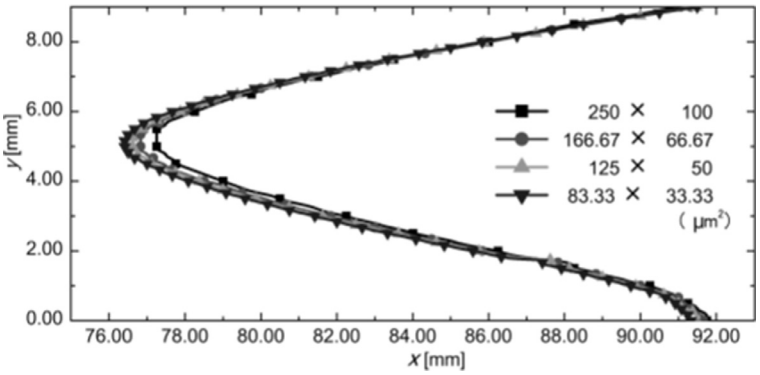

Fig. 4. Grid dependency of V-shaped deflagration front.

ture. A line on the right upper corner corresponds to the height of $H = Hs$. Initiation of the deflagration receded slightly downstream due to the difference of the reaction mechanism employed. However, the transition pattern, the distribution of temperature and pressure, and the wave angles of OSW and ODW were almost coincident. The smooth-transition of the inflow (A) was reproduced with 35.79° OSW and 44.00° ODW (36.00° OSW and 44.00° ODW in the numerical study by Da Silva and Deshaies, and 35.50° OSW and 45.50° ODW in their shock/detonation polar analysis respectively), and the abrupt-transition of the inflow (B) was reproduced with 30.60° OSW and 40.40° ODW (41.00° ODW in the numerical study by Da Silva and Deshaies and 42.00° ODW in their polar analysis, without a statement on the quantitative OSW angle.

3.2. Grid dependency evaluation

As will be discussed later, V-shaped deflagration front appeared in Case A-6, which is one of the most characteristic features observed in this study. Simulations of the case using different resolutions were conducted to evaluate the sensitivity of the strucutre of ODW. Resolution of extended grid (12.50 cm × 3.00 cm) was varied among $(\Delta x \times \Delta y =) 250 \times 100\,\mu m^2$, $166.67 \times 66.67\,\mu m^2$, $125 \times 50\,\mu m^2$ (the present one), and $83.33 \times 33.33\,\mu m^2$. The result is shown in Fig. 4 as the dependency of the location of V-shaped deflagration front which was proved to exhibit the strongest dependency in the whole structure. The $250 \times 100\,\mu m^2$ grid shows a relatively large deviation on the apex of the flame, but the more refined grids all predicted similar locations, which proves a negligible influence of the resolution on the structures being studied.

3.3. Non-uniform conditions

The non-uniform conditions described by Eq. (1) listed in Table 1 were simulated. The distributions of pressure indicating the shock fronts and water mass fraction indicating the flame fronts are illustrated in Fig. 5 as overlaid contours. There are several oblique lines in the left-upper side, denoting the incoming local equivalence ratio and the $H = Hs$ line respectively.

Case A-1 (Fig. 5(a)) with $\varphi_0 = 1.50$ noticeably receded the deflagration front from the uniform condition (Fig. 3(a)). Increase of the OSW angle at the transition also became a little discontinuous, but the existence of the triple point is still unclear in the figure. ODW downstream

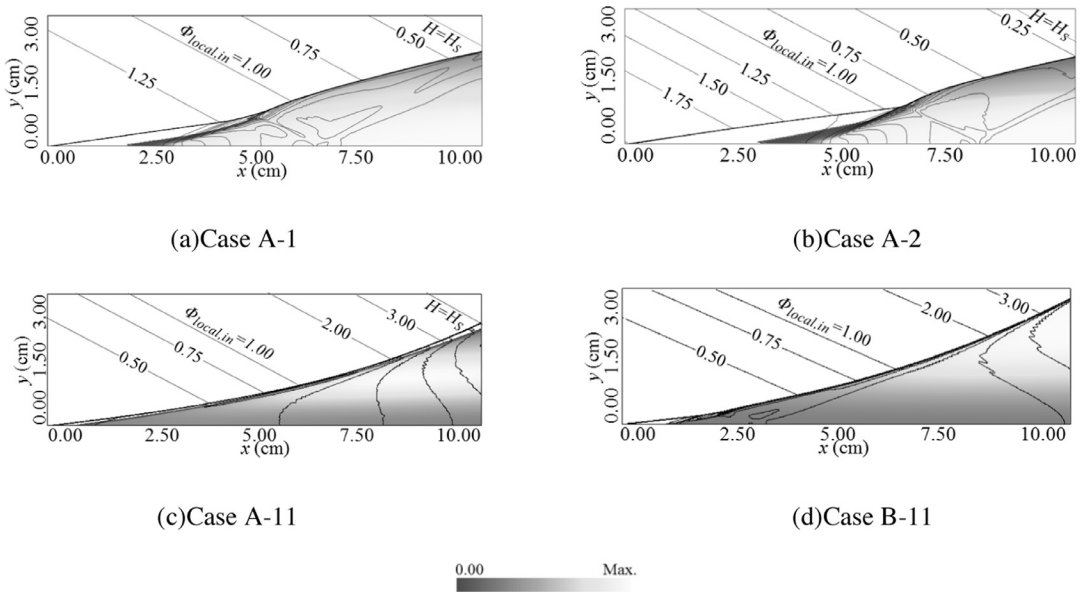

Fig. 5. Overlaid contours of pressure (black) and water mass fraction (gray–white) as the computational results using standard grid (10.00 cm × 3.00 cm).

of the transition forms a convex front. These changes are attributed to two non-uniformities: one is variable induction time by non-uniform equivalence ratio, and the other is variable incoming Mach number. The latter has been considered as the main cause of the deformation of ODW by other researchers [19–21]. However, we previously reported the notable effects of the former when φ_0 exceeds around 3.50 [34]. Therefore, although the former effect should be weaker in weakly non-uniform conditions displayed in Fig. 5, but it should not be true for the stronger non-uniformities. When the non-uniformity increases to that of Case A-2 (Fig. 5(b)) where $\varphi_0 = 2.00$, a more discontinuous increase of the shock angle leads to the emergence of the triple point. Reflection of the compression waves to the surface of the wedge generates a somewhat discontinuous change, which resembles λ-shaped structure studied by Teng et al. [18]. OSW also started to exhibit a positive curvature.

The center-lean conditions showed similar changes, among which the observed structures in Case A-11 and Case B-11 are illustrated in Fig. 5(c) and (d). In these conditions, the deflagration front progressed forward on the contrary to our expectation, due to the stronger effect of the larger incoming Mach number creating the stronger OSW than that of a less reactive composition. This tendency was retained in all the cases where $\varphi_0 < 1.00$. The incident shock deformed into a concave shape, and the abrupt-transition of the inflow (B) was replaced by the smooth-transition. In addition, it should be also noted that the shock front and the flame front remain fully coupled in Case B-11 even on the outlet boundary, while the ODW in Case A-11 experiences decoupling downstream around $x = 8.50$ cm.

3.4. V-shaped deflagration front

More strongly center-rich conditions receded ODW front so that it became difficult to discuss it with standard grid. grid was then used to simulate Cases A-4–A-9, and Case B-1. Figure 6 illustrates the overlaid contours in the same way as Fig. 5 does.

Cases A-4–A-9 (Fig. 6(a)–(c)) exhibited a fundamental change to the structure of ODW: the deflagration front transformed into a V-shaped one. The leading edge of it is located away from the surface of the wedge due to a less reactive mixture there.

As a result of the emergence of V-shaped deflagration front, another important structural change appered: second triple point behind the orginal one became evident on ODW front (in Case A-4, Fig. 6(a)) or decoupled OSW (in Case A-5, Fig. 6(b)). Emergence of the second triple point can be attributed to V-shaped flame as indicated in the pressure contours and depicted in a schematic picture in Fig. 7: compression waves are generated not only on the upper side of the deflagration front (as is observed in the uniform conditions, Fig. 1), but also on the lower side of it. They accumulate onto the surface, where a distinct shock is generated, reflecting from there and eventually intersecting with the incident front.

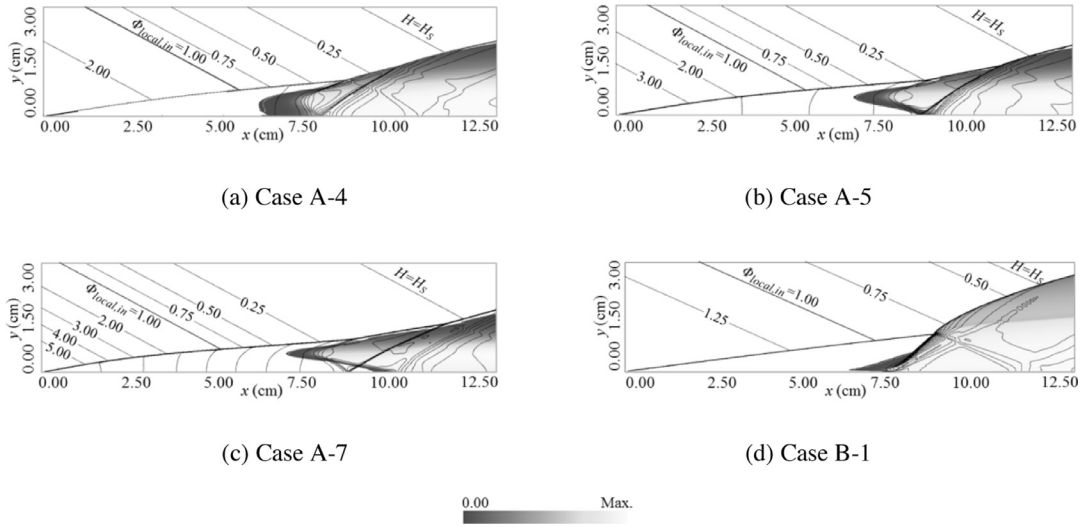

Fig. 6. Overlaid contours of pressure (black) and water mass fraction (gray–white) as the computational results using extended grid (12.50 cm × 3.00 cm).

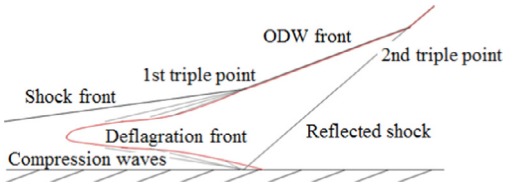

Fig. 7. Schematic picture of V-shaped flame and the second triple point.

Increase of OSW angle or ODW angle on the second triple point further intensifies the original ODW front or causes re-transition. However, in Case A-7 (Fig. 6(c)), no transition occurs on both triple points. It results in a full SIC with the triple points simply appearing as the intersections of the triple inert shocks.

On the other hand, the structures observed in Cases B-1–B-9 proved to have a stronger sensitivity to the non-uniformity than it did in Cases A-1–A-9; The weakest non-uniformity in Case B-1 receded the deflagration front greatly (Fig. 6(d)). However, the general structure in Case B-1 did not change from that of the uniform condition (Fig. 3(b)). Because the stronger non-uniformities further receded the flame front, the changes encountered in Cases B-2–B-9 will be addressed using largest grid.

3.5. V + Y Mach stem

Largest grid was used to compute Cases B-2–B-9 to capture the largely receded structures. They were illustrated in Fig. 8. Case B-2 (Fig. 8(a)) encountered V-shaped flame and the incidental second triple point as observed in Cases A-4–A-9. However, differently from them, the downgoing compression waves concentrate into the shock before they reach the surface. As a consequence, the regular reflection of the shock occurs on the surface.

When the non-uniformity was increased to that of Case B-4 (Fig. 8(b)), the reflection changed into a Mach stem. As a result, the combined structure of V-shaped flame and the Mach stem resembled 'V + Y' in its shape. Therefore, we term this structure 'V + Y Mach stem'. This structure can be explained similarly as can be done for V-shaped flame, which is depicted in Fig. 9.

In Case B-6 (Fig. 8(c)), the Mach stem became distorted to have curvature due to a stronger influence of the variable incoming Mach number. The ODW front as well as V + Y Mach stem was retained fully coupled in the parameters presently studied, which proved that intensive combustion and stabilization of ODW were promised even under the strong non-uniformity.

3.6. Analyses on V-shape

The position of the flame leading edge in each case was summarized in Fig. 10(a) as the relationship with φ_0. The black and white plots correspond to Case A- and B-, respectively. The shape of each plot denotes the flame geometry obtained. The number under the triangle and square plots is the incoming local equivalence ratio to V-apex. As was indicated in Figs. 6 and 8, V-shaped flame always appears at an almost constant location regardless of the magnitude of the non-uniformity, while the up-facing flame experiences a large variation. The center-lean conditions encounter the flame more

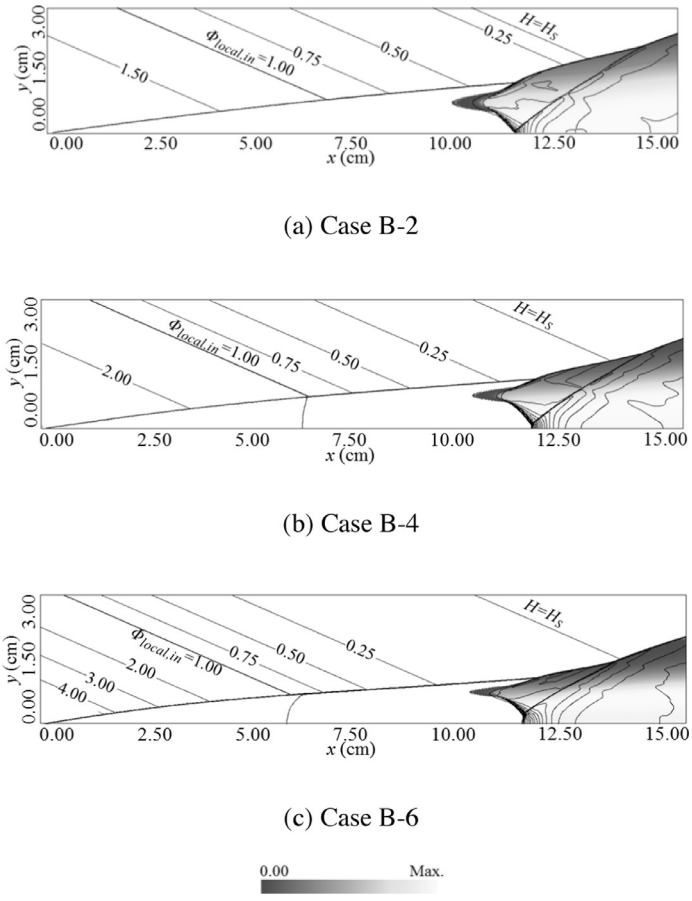

Fig. 8. Overlaid contours of pressure (black) and water mass fraction (gray–white) as the computational results using largest grid (15.00 cm × 3.00 cm).

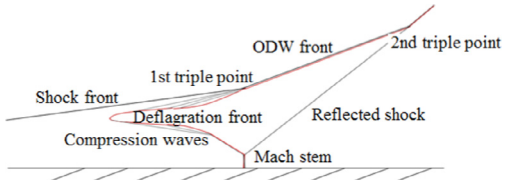

Fig. 9. Schematic picture of V + Y Mach stem.

upstream with a relatively minor variation. It is as important to note that the streamline into V-apex has a similar local equivalence ratio value (1.76–2.06 in Case A- and 0.85–1.13 in Case B-). This constant thermochemical property enables the leading edge to be located in a similar position, even though V + Y Mach stem progressed a little forward at φ_0 = 8.00 (Case B-9).

Finally, we discuss and suggest the threshold for whether V-shape appears or not from an analytical perspective. A simple consideration of the geometry around V-shaped flame front leads to a relation $\mathrm{d}x_{\mathrm{flame}}/\mathrm{d}y = \mathrm{d}x_{\mathrm{shock}}/\mathrm{d}y + \mathrm{d}l_{\mathrm{ind}}/\mathrm{d}y < 0$ on the lower side of it on the assumption of the parallel post-shock flow along the wedge. Since $\mathrm{d}x_{\mathrm{shock}}/\mathrm{d}y = 1/\tan(\beta-\theta)$, this can be reduced as below

$$g = -\tan(\beta-\theta)\mathrm{d}l_{\mathrm{ind}}/\mathrm{d}y > 1 \qquad (2)$$

where g is defined as the induction length gradient factor. If Eq. (2) is satisfied somewhere close to the wedge, a down-facing flame front should be formed there. Therefore, it can be concluded that V-shape should appear when the maximum value $g_{\max} > 1$. Then, we combined Rankine–Hugoniot relations across the inert shock with 0D isochoric combustion simulation behind it to calculate $g_{\max}$ in each case, using only the information available beforehand (without 2D numerical results): the inflow properties and the concentration gradients (Eq. (1)). The calculated results were summarized in Fig. 10(b). All the cases except one case (Case A-4 with φ_0 = 3.00) actually encounter V-shape at

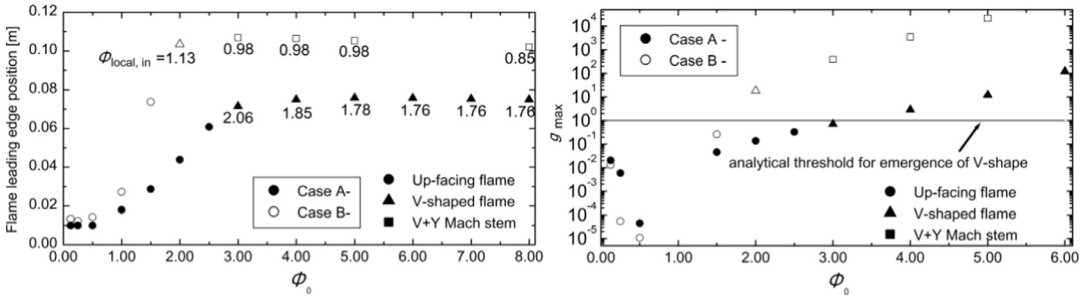

(a) Flame leading edge position (b) Induction length gradient factor g

Fig. 10. Properties of the flame front versus the centerline equivalence ratio.

the value of g_{max} above unity. Inconsistency in Case A-4 can be attributed to the deviation from the isochoric and parallel flow due to the non-uniform post-shock pressure causing subsequent compression and expansion. However, its g_{max} value is still around the analytical threshold, which validates the above method as reasonable for generalizing the V-shape emergence.

4. Conclusion

In our study, effects of the non-uniform premixing of a hydrogen–air mixture on wedge-stabilized oblique detonation were addressed through a parametric numerical study using two-dimensional Navier–Stokes equations with a detailed chemical kinetics. A concentration gradient was artificially described by the Gaussian function.

The computational results obtained uncovered several new features: when a fuel-rich condition occurs on the centerline, the abrupt-transition occurs with the emergence of the triple point. In the stronger concentration gradients, V-shaped flame appears, generating the second triple point on the incident front due to the downgoing compression waves emanating on the lower side of it. This second triple point sometimes induced re-transition to ODW, which intensified combustion behind it. V + Y Mach stem also appeared in a steeper concentration gradient as a combination of V-shaped flame and a Y-shaped Mach stem attached on the surface. On the other hand, when a fuel-lean condition occurs on the centerline, the flame leading edge progressed forward due to a larger incoming Mach number and the abrupt transition was replaced by the smooth one, but without any evidence of V-shape. The apex of V-shaped flame was always located in a similar location along the streamlines within a narrow range of incoming equivalence ratio, which will promise a well-stabilized flame in the ODWE combustor. A geometrical analysis revealed that the threshold for emergence of these V-shapes can be reasonably attained by the magnitude of induction length gradient close to the wedge. This analytical method should therefore be also useful for prediction of V-shape in the inflow conditions not yet studied.

ODW with unstable transversal waves [10–12] will be of a great concern in our future works since the effects of the non-uniformity on it are considered to be significant, as was confirmed against normal detonation wave [22–24].

References

[1] R.A. Gross, *AIAA J.* 1 (5) (1963) 1225–1227.
[2] S.A. Ashford, G. Emanuel, *Shock Waves* 3 (4) (1994) 327–329.
[3] J.A. Nicholls, E.K. Dabora, in: The International Symposium on Combustion, The Combustion Institute, 1961, pp. 644–655.
[4] R. Dunlap, R.L. Brehm, J.A. Nicholls, *Jet Propuls.* 28 (7) (1958) 451–456.
[5] P. Wolanski, *Proc. Combust. Inst.* 34 (1) (2013) 125–158.
[6] G.P. Menees, H.G. Adelman, J.L. Cambier, J.V. Bowles, *J. Propuls. Power* 8 (3) (1992) 709–713.
[7] H.F. Lehr, *Astronaut. Acta* 17 (1972) 589–597.
[8] C. Li, K. Kailasanath, E.S. Oran, *Phys. Fluids* 6 (4) (1994) 1600–1611.
[9] L.F.F. da Silva, B. Deshaies, *Combust. Flame* 121 (2000) 152–166.
[10] J.-Y. Choi, D.-W. Kim, I.-S. Jeung, F. Ma, V. Yang, *Proc. Combust. Inst.* 31 (2007) 2473–2480.
[11] J.-Y. Choi, E.J.-R. Shin, D.-R. Cho, I.-S. Jeung, V. Yang, Forty Sixth AIAA Aerospace Sciences Meeting and Exhibit, Aerospace Sciences Meetings, AIAA, Nevada, AIAA 2008-1032, 2008.
[12] J. Verreault, A.J. Higgins, R.A. Stowe, *Proc. Combust. Inst.* 34 (2013) 1913–1920.
[13] A. Matsuo, K. Fujii, *AIAA J.* 34 (10) (1996) 2082–2089.
[14] R.L. Alpert, T.Y. Toong, *Astronaut. Acta* 17 (1972) 539–560.
[15] J. Verreault, A.J. Higgins, *Proc. Combust. Inst.* 33 (2011) 2311–2318.
[16] S. Maeda, J. Kasahara, A. Matsuo, *Combust. Flame* 159 (2012) 887–896.
[17] Y. Liu, Y.-S. Liu, D. Wu, J.-P. Wang, *Shock Waves* 26 (2) (2015) 327–329.

[18] H. Teng, Y. Zhang, Z. Jiang, *Comput. Fluids* 95 (2014) 127–131.
[19] J.L. Cambier, H. Adelman, G.P. Menees, *Jet Propuls.* 6 (3) (1990) 315–323.
[20] V.V. Vlasenko, V.A. Sabel'nikov, *Combust. Explos. Shock Waves* 31 (3) (1995) 376–389.
[21] J.P. Sislan, R. Dudebout, J.M. Schumacher, T. Islam, J. Redford, *Propuls. Power* 16 (1) (2000) 41–48.
[22] K. Ishii, M. Kojima, *Shock Waves* 17 (2007) 95–102.
[23] K.G. Vollmer, F. Ettner, T. Sattelmayer, *Combust. Sci. Technol.* 184 (2012) 1903–1915.
[24] M.S. Kuznersov, V.I. Alekseev, S.B. Dorofeev, I.D. Matsukov, J.L. Boccio, in: The International Symposium on Combustion, The Combustion Institute, 1998, pp. 2241–2247.
[25] G.P. Menees, H.G. Adelman, J.L. Cambier, NASA TM-102839, 1991.
[26] Y.W. Wang, J.P. Sislian, *J. Propuls. Power* 26 (5) (2010) 1114–1124.
[27] A.A. Konnov, *Eurasian Chem. Technol. J.* 2 (2000) 257–264.
[28] H.C. Yee, NASA TM-89464, 1987.
[29] B. Poling, J. Prausnitz, J. O'Connell, *The Properties of Gases and Liquids*, fifth ed., McGraw-Hill, New York, U.S., 2001 9.1 - 10.68.
[30] M.O. Connaire, H.J. Curran, J.M. Simmie, W.J. Pitz, C.K. Westbrook, available at https://combustion.llnl.gov/archived-mechanisms/hydrogen.
[31] A. Jameson, S. Yoon, *AIAA J.* 25 (7) (1987) 929–935.
[32] Y. Ju, *AIAA J.* 33 (8) (1995) 1418–1425.
[33] R.A. Gross, W. Chinitz, *J. Aerosp. Sci.* 27 (7) (1960) 517–524.
[34] K. Iwata, S. Nakaya, M. Tsue, in: Twenty Fifth International Colloquium on the Dynamics of Explosions and Reactive Systems, IDERS, Leeds, U.K., 2015.